Effects of plasma current on nonlinear interactions of ITG turbulence, zonal flows and geodesic acoustic modes

P. Angelino[1], A. Bottino[2], R. Hatzky[2], S. Jolliet[1], O. Sauter[1], T.M. Tran[1], L. Villard[1]

[1]Centre de Recherches en Physique des Plasmas,
Association Euratom Confédération Suisse,
EPFL, Lausanne, Switzerland

[2]Computer Center of the Max-Planck-Gesellschaft and
the Institute for Plasma Physics,
D-85748 Garching, Germany

September 1, 2005

Abstract

A class of small scale drift waves, the microistabilities, are generally held responsible for the phenomenon of anomalous transport observed in magnetic confinement fusion experiments. The magnitude of this transport depends on the turbulence state resulting from nonlinear saturation mechanisms. For electrostatic perturbations, several gyrokinetic and gyrofluid simulations have shown that, as microinstabilities develop, nonlinear coupling creates a 'zonal' $E \times B$ component which has a stabilizing effect on turbulence. In toroidal systems, zonal flows show an oscillatory behavior due to coupling with poloidally asymmetric perturbations. These oscillations are called geodesic acoustic modes (GAMs), the coupling coming trough the geodesic curvature. Simulations show a dependence of GAMs on the safety factor q, zonal flow oscillations being more important in high q regions than in low q regions. This affects the turbulent transport because the oscillatory zonal flows are less effective in suppressing the turbulence than the slowly time varying ones. We present results from the global nonlinear electrostatic gyrokinetic code ORB5. Particular attention is devoted to give new insight of the mutual interactions between toroidal ion temperature gradient modes (ITGs), zonal flows and GAMs in realistic tokamak magnetohydrodynamic equilibria. A q value scan at constant shear has been performed, showing an anomalous heat flux decreasing with increasing plasma current. As the total plasma current is increased, GAM oscillations are suppressed. The stationary zonal flows, thus obtained, lead to a substantial reduction of the radial heat flux. Effects of the q profile are also investigated.

1 Introduction

In all tokamak experiments, the particle and heat losses greatly exceeds the theoretical predictions based on neoclassical theory. In the neoclassical model, binary collisions are the basic mechanism by which energy and particles are transported across the magnetic field lines. Although the reason for the difference between the measured radial transport and the neoclassical prediction is not yet completely understood, the main source of anomalous transport is now mainly attributed to plasma turbulence [1] driven by free energy sources in the plasma. These small scale plasma fluctuations arise from instabilities driven by temperature and density gradients always present in any magnetic confinement device. These instabilities are often called microinstabilities because they are characterized by small spatial scales as compared to the size of the tokamak (but large compared to the Debye length above which the plasma is quasi-neutral) and by low frequencies as compared to the plasma frequency, ω_{pe}. The physics governing plasma turbulence is extremely complex because of the wide range of spatial and time scales involved in the collective turbulent motion of plasma particles. Therefore, a comprehensive theoretical model for anomalous transport does not exist yet which can explain the high heat conductivity found in the experiments. Most existing transport models are based on a mixing length rule based on linear instability theory. The fact that the nonlinear processes rather than linear quantities determine the scaling of the ion heat conductivity places considerable limitations on the applicability of these models. The ion heat anomalous transport in the plasma core seems to be dominated by a class of microinstabilites, the toroidal ion temperature gradient (ITG) driven modes [2]. ITG turbulence is known to self organize to form coherent macroscopic structures [3]. This structures takes the form of a macroscopic electrostatic potential which depends only on the radial coordinate. The $E \times B$ poloidal flows associated to this potential are referred as zonal flows. Both experimental [4] and theoretical evidences [5] have been supplied which demonstrate that zonal flows play a crucial role in regulating the nonlinear evolution of ITG turbulence. This effect relies on the capabilities of the zonal flows to shear the radial coherent turbulence structure. Introducing the flux surface average of the electrostatic potential, $\overline{\phi}$, and the magnetic coordinates ψ and φ, the shearing rate, $\omega_{E\times B} = \frac{\Delta\psi}{\Delta\varphi}\frac{\mathrm{d}^2}{\mathrm{d}\psi^2}\overline{\phi}\,(\psi)$, is a measure of the shearing action of the zonal flows on the global mode structure. When $\omega_{E\times B}$ becomes comparable to the decorrelation rate of the ambient turbulence, this one is strongly suppressed.

In toroidal system such as tokamak, an important feature of zonal flow is that they can oscillate in time by coupling with poloidally asymmetric (m,n)=(1,0) pressure perturbation [6]. These oscillations are called the geodesic acoustic modes (GAM) since the coupling comes though the geodesic curvature. The importance of GAM oscillation resides in the different shearing efficiency zonal flows have, in relation to their oscillatory behavior. While the stationary zonal flows suppress the turbulence efficiently, fluctuations makes the suppression of the turbulence by the zonal flows less effective. In order to take into account this effect an effective shearing rate $\omega_{Eff} \lesssim \omega_{E\times B}$ has been introduced [7]. Recently, it has been pointed out [8] that the zonal flow behavior shift between stationary and oscillatory is regulated by the value of the safety factor q_s. All these arguments suggest that a series of relationships can be established be-

tween turbulence, zonal flow, GAM and q_s, which depends on its turn on the plasma current profile. To investigate these interactions we have run a series of numerical simulations with the global nonlinear gyrokinetic code ORB5. The results are illustrated in the present work.

The paper is organized as follows. The model and its implementation in the numerical code ORB5 is described in Sec. 2. The magnetic equilibrium and the parameters of the simulations are presented in Sec. 3. The heat flux and ion conductivity are analyzed in Sec. 4. Sec. 5 gives a detailed description of the heat flux modulation by the zonal flows. The effects of GAM oscillations on turbulent transport are investigated in Sec. 6. The results are summarized in Sec. 7.

2 The model

The simulation are based on the electrostatic gyrokinetic equations derived by Hahm [9]. In the code ORB5 [10] ion motion is described by means of the non linear gyrokinetic Vlasov equation. An adiabatic model is used for electrons, where the flux surface averaged part of the potential as been subtracted in order to obtain the correct zonal flow amplitude [11]. The system is closed by the Poisson equation, that, in the long wavelength approximation, reduces to the linearized ($n_i \simeq n_0 + \delta n$) quasi neutrality equation. This set is proofed to be energy conserving [12]. A finite element scheme (FEM) is used for the solver. The five dimensional particle phase space is sampled with a Particle In Cell (PIC) scheme, and a control variate (δf) method is used in order to reduce noise [13]. A canonical Maxwellian is used as equilibrium distribution function in order to avoid spurious drive of zonal flow [14]. No assumption is made on the toroidal magnetic equilibrium. ORB5 is interfaced with the code CHEESE [15], which supplies real MHD equilibria or experimental magnetic configuration reconstruction.

3 Simulation parameters

The analysis, presented in this paper, is based on a series of five simulations where the total plasma current has been varied in five step: 1, 1.3, 1.6, 2 and 2.3 times a basic value of $I_0 = 9.3 \cdot 10^4\ A$. Since [16]:

$$q(a) = \frac{2\pi a^2 B_\phi}{\mu_0 I_p R} \tag{1}$$

varying the total current I_p, and keeping constant the other parameters, is equivalent to rescaling the safety factor profile plotted in 2. We label this simulations as 1x, 1.3x, 1.6x, 2x and 2.3x according to the total current value. The basic magnetic configuration is the one reconstructed from shot 22516 of the tokamak TCV. It is an elongated D-shaped plasma (fig. 1), with inverse aspect ratio $\epsilon \equiv a/R = 0.27$, $a = 0.24\ m = 40\ \rho_i$. The value of the magnetic field on axis is $B_0 = 1.44\ T$. Starting from this configuration, some parameter has been retuned to destabilize ITG (Ion Temperature Gradient) modes, since global linear simulations with experimental temperature and density profile showed that the ITG mode is marginally stable in shot 22516 [17]. The ion temperature

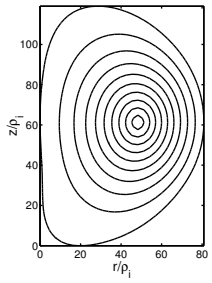

Figure 1: Magnetic equilibrium: poloidal section showing the magnetic surfaces, r and z are the polar coordinates in units of the ion gyroradius ρ_i.

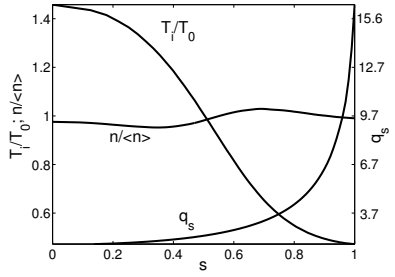

Figure 2: Effective initial density n and ion temperature T_i profiles. Safety factor q_s profile. Density is normalized to its averaged value $< n >$. Ion temperature is nomalized to the value T_0 at $s = 0.5$.

gradient has been increased, and the effective profile obtained is shown in fig. 2. Electron temperature profile is flat, with $T_e = T_i\,(s_0 = 0.5)$, and the effective initial density $n_{i0} = n_{e0}$ is plotted in fig. 2.[1] In order to simplify the analysis, constant null pressure is assumed. The numerical simulation have been performed with 33 millions of tracers. The field is solved on a grid 64×128×64, in toroidal coordinate s, θ, φ ($s = \rho/a$ is the normalized radial coordinate). A Fourier filter is applied: $-40 \leq m \leq 40$ and $0 \leq n \leq 15$ (here m, n are respectively the poloidal and toroidal wave numbers). The chosen time step is $\Delta t \Omega_{ci} = 5$. The ion species considered are hydrogen.

4 Heat flux analysis

A global quantity, very useful in characterizing our simulations, is the radial averaged heat flux. Fig. 3 shows its time evolution for the five different values of the total current. The five curves show a similar behavior, with a transient

[1] We talk here of 'effective' profile. Since the initial distribution function is a canonical Mawellian, the input analitic profile is given as a function of the toroidal canonical momentum ψ_0. It obviously differs from a radial profile given as a function of $s = \sqrt{\psi/\psi_s}$, where ψ is the poloidal magnetic flux, and ψ_s is its value at the plasma boundary. Thus, 'effective' density and temperature profiles are reconstructed from the distribution function and the velocities of the particles at time $t = 0$.

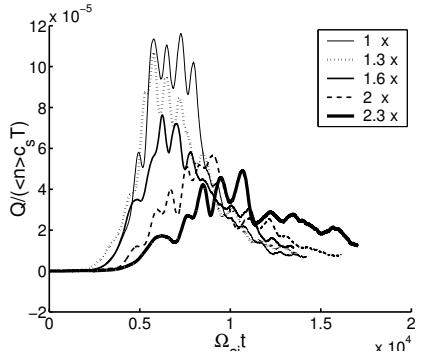

Figure 3: Radial average heat flux, time history for the different current values.

phase following the initial linear one, characterized by a series of bursts typical of an avalanche like behavior. After this transient phase, a saturated, turbulent equilibrium take place. The time scale of the evolution of the heat flux differs from one simulation to another. In order to make physically significative comparisons, we need to choose physically equivalent times on the five curves. For this purpose, we choose two point on each curve: the highest peak position in the transient phase and the beginning of the saturated phase. These are the basis points of our analysis.Since temperature and density profiles are free to evolve and they do evolve differently in each run, we introduce a more transport relevant quantity, the ion conductivity χ_i, which accounts also for the variations of these profiles. If Q is the heat flux, χ_i is defined as[16]:

$$\chi_i \equiv -\frac{Q}{n_i \nabla T_i} \tag{2}$$

In the following, we will refer to his value normalized to the gyro-Boom transport coefficient [18]:

$$\chi_{gB} = \frac{\rho_i^2 c_s}{\langle a \rangle} \sim \frac{\rho_i^2 c_s}{a\sqrt{\kappa}} \tag{3}$$

where c_s is the sound speed, $\langle a \rangle$ is the averaged minor radius, and $\kappa = 1.5$ is the plasma elongation.

We start analyzing the peak values of Q and χ_i, averaged over the plasma minor radius. Fig. 4 and 5 show a linear dependence of the two quantities on the inverse of the total current. The same dependence can be found in the values of χ_i after the turbulence saturation, fig. 6. In this figure, the scattering of the points on the plot is larger compared to fig. 5. This scattering is due to the fluctuations in χ_i in the saturated phase, which makes it difficult to compare its value across the simulations. To partly overcome this problem, the values plotted on fig. 6 represent an average over 500 Ω_{ci}^{-1} (where Ω_{ci} is the ion cyclotron frequency). This time interval is the typical period of these oscillations.

Linear simulations have been run on the same equilibrium with the global linear gyrokinetic PIC code GYGLES [19]. The linear value for χ_i is estimated using a mixing length argument. In its simplest form, the mixing length estimate of diffusion coefficients consists of approximating the spatial correlation length

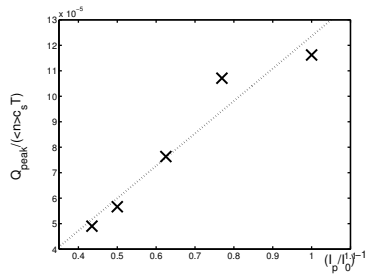

Figure 4: Radial averaged heat flux at peak position, as a function of inverse total current.

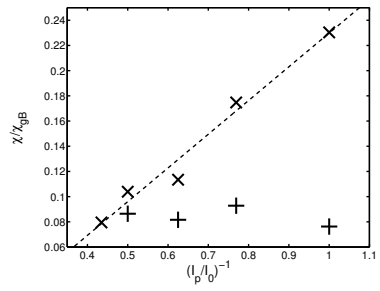

Figure 5: Radial averaged χ_i/χ_{gB} at peak position, as a function of inverse total current. Plus signs reprensent the results from linear calculation, while cross signs are results from the nonlinear one. Linear results are scaled down by a factor 5.5 to better fit in the graph.

and time fluctuation of the turbulent state with the typical perpendicular scale length ($k_\perp^{-1}$) and the linear growth rate (γ) of the most unstable mode:

$$\chi_i \simeq \frac{\gamma}{k_\perp^2} \tag{4}$$

The results are plotted on fig. 5. This results do not show any clear relationship between the total current and χ_i, suggesting that the phenomenon we are investigating is of nonlinear nature. In order to understand this nonlinear phenomenon, we move on studying the behavior of zonal flow.

5 Zonal flow analysis

While ITG turbulence evolve from the initial linear phase to a nonlinear stage, zonal flows are generated. In the nonlinear stage, two regimes can be identified. In a first time, a series of bursts in the heat flux can be observed, later, a turbulent equilibrium is set on place. In both phases there are evidences of a strong correlation between the heat flux and the zonal flows. In this section, we restrict the analysis to the case with 1x total current, since the features we will describe are common to all the five current cases. We start from the burst regime, a detailed picture of this phase is give by fig. 7, and we focus on the radial position $s = 0.5$, where the temperature gradient has its highest value.

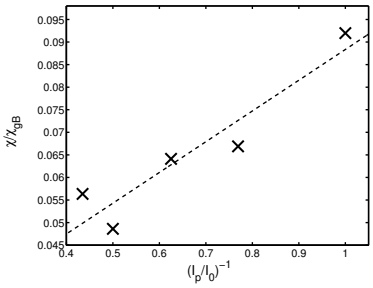

Figure 6: Radial averaged χ_i/χ_{bB} after saturation, as a function of inverse total current.

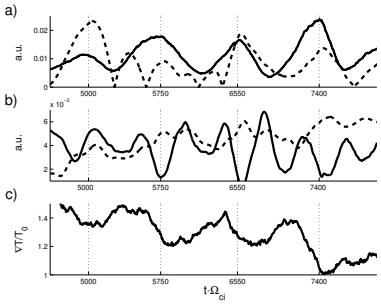

Figure 7: a) time evolution of χ_i (solid line), and shearing rate absolute value (dashed line) at radial position $s = 0.5$, during the burst phase. b) Radial averaged $E \times B$ velocity (dashed line) and its abslotue value (solid line). c) Temperature gradient at $s = 0.5$. Quantities in plot a) and b) are in arbitrary unit, while the temperature gradient is normalize at the initial temperature $T_0(s = 0.5)$.

From plot 7.a and 7.c, the heat flux or ion conductivity χ_i peaks correspond to local flattening and peaking in the radial temperature profile. This is characteristic of an avalanche like regime. The temperature gradient locally peaks until an avalanche is triggered, and, locally, the ITG turbulence grows exponentially. The associated heat transport then flattens the temperature gradient and the turbulence is reduced. Then the temperature gradient peaks again and another avalanche is triggered. The sequence continues until there is enough free energy to maintain it. Indeed, after each burst, the temperature gradient relax until it reach a level it cannot drive avalanches anymore. The system has reached a new turbulent equilibrium. In this picture, the zonal flow oscillations in fig. 7.c are driven by the turbulence oscillations. If this is the mechanism underlying the burst sequence, reducing the initial temperature gradient under a certain critical value should make the bursts disappear. In fact a set of simulations run to check this point shows that a lower gradient reduce the burst amplitude but doesn't eliminate them. Moreover, in the case where the zonal flow are artificially suppressed (by Fourier filtering the mode $n = 0$ in the electrostatic potential), the bursts are suppressed too. This suggest a different explanation of the phenomenon. Lets consider the effective shearing rate of the $E \times B$ velocity [7], which is also plotted on fig. 7.a. In the burst phase the ITG turbulence grow until the shearing rate exceeds the ambient turbulence decorrelation

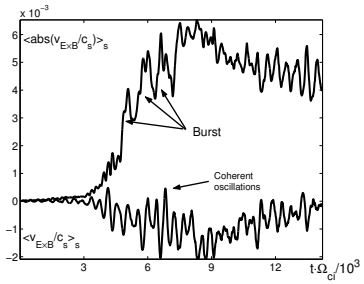

Figure 8: Radial averaged $E \times B$ velocity (lower line) and its abslotue value (upper line) as a function of time. Velocities are normalized to the soud speed c_s and time is normalized to Ω_{ci}.

rate. ITG turbulence and associated transport are then significantly reduced. Now we should need a damping mechanism for the zonal flows, in order for the shearing rate to decrease below the decorrelation rate. At this point, ITG turbulence could grow again and start a new burst. But, zonal flow are not dumped by collisionless processes (Landau damping) [20]. Nevertheless, $E \times B$ velocity oscillations, like GAM, can bring the shearing rate below the needed level, and, together with a peaking in the temperature gradient, it can allow for the ITG turbulence to grow again. The sequence is anyway maintained (like in the avalanche like picture) by the temperature gradient, when the profile relaxation brings the gradient under the critical value, the ITG modes become marginally stable and the system comes to a turbulent equilibrium. This burst behavior is similar to the one found in presence of collisions [21]. But, here, the zonal flow modulation comes from GAM oscillations instead than from a collisional dumping.

Bursts observed in zonal flows have a non coherent radial structure. But on top of these, zonal flows have other fluctuations with a coherent radial structure. The two kind of oscillations can be separated plotting the radial average of $E \times B$ velocity and of its absolute value 8. In the first plot, the radially non coherent structures cancel out, showing the coherent oscillations. In the second plot the bursts are instead visible. In the turbulent equilibrium phase, the coherent fluctuations become more important and they dominate the $v_{E\times B}$ velocity. Heat flux does not respond directly to this oscillation fig. 9, but nevertheless they have a major influence on the transport level. This aspect will be investigated in details in the next section.

6 GAM analysis

A spectral analysis has been performed in order to evaluate the frequency of the coherent fluctuations in the averaged $v_{E\times B}$ velocity. A time interval of 2560 Ω_{ci} as been chosen for the Fourier transform, starting at the beginning of the saturated phase of each total current case. The found value, $0.011 \pm 0.003\ \Omega_{ci}$, is the same in four simulations and it correspond to the geodesic acoustic mode frequency. Indeed, an expression for GAM frequency is given in [8], which, converted in unit of Ω_{ci}, becomes $\omega_{GAM} \simeq c_s/R \simeq 0.011\ \Omega_{ci}$. The predicted

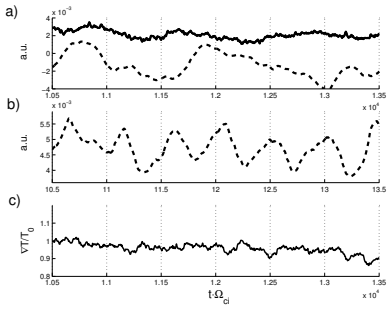

Figure 9: a) time evolution of χ_i (solid line), and shearing rate absolute value (dashed line) at radial position $s = 0.5$, during the burst phase. b) Absolute value of the radial averaged $E \times B$ velocity. c) Temperature gradient at $s = 0.5$. Quantities in plot a) and b) are in arbitrary unit, while the temperature gradient is normalize at the initial temperature $T_0(s = 0.5)$.

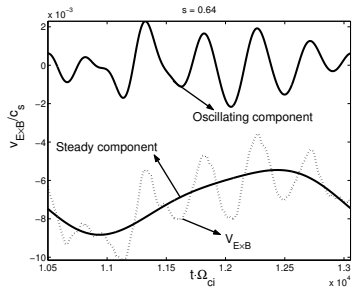

Figure 10: $E \times B$ velocity at radial position $s = 0.7$. The full signal is plotted with a dashed line, while upper and lower solid lines are, respectively, the component oscillating at the GAM frequency and the steady one. Values are normalized to the sound speed c_s.

value, as the one found numerically doesn't depend on the rotational transform, and correspondingly on the total current. The only exception is the run 1.3x. Here the frequency found is twice the one of the other cases, showing that the plasma can oscillate also at the second GAM harmonic.

To study the GAM amplitude, we applied a Fourier filter on the $v_{E\times B}$ velocity signal, in order to separate the steady part, from the oscillatory part. The results are plotted in fig. 10. The GAM amplitude is then evaluated taking the average of the peak to bottom difference over a series of oscillations. In fig. 11 we plotted the averaged value of the steady component and the averaged GAM amplitude as a function of the normalized radial coordinate s.We remark that the radial dependence of the GAM amplitude which follows the safety factor q_s. In reference [8], global Landau-fluid simulations are presented showing that the zonal flow behavior changes as a function of the safety factor q_s. According to the equations derived in the same reference, $(m, n) = (1, 0)$ pressure perturbations drive come from three terms. One is a nonlinear coupling with turbulence, the second is the coupling with zonal flows through geodesic curvature (GAM term), and the third is a coupling with sound waves (sound wave term). This

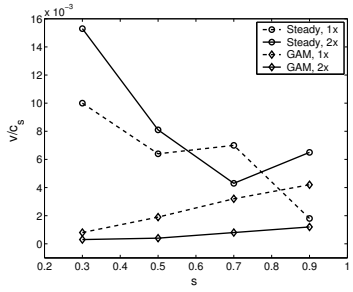

Figure 11: Averaged value of the steady component (circles) and the GAM amplitude (diamonds) as a function of the normalized radial coordinate s. The dashed line shows results from 1x simulation, and solid line from 2x simulation. Values are normalized to the sound speed c_s.

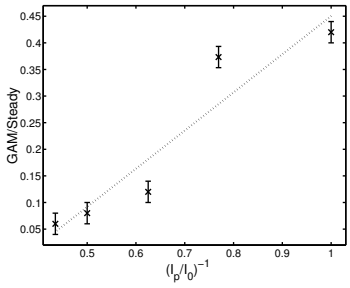

Figure 12: Rate of the averaged GAM amplitude (G) and the steady zonal flow component (S) as a function of inverse total current.

term is opposite to the GAM one and inversely proportional to q_s, so at low q_s it becomes large and can balance the GAM term, preventing the excitation of the $(1,0)$ pressure mode by the zonal flow. At high q_s, where the sound wave term is negligible, zonal flows can excite $(1,0)$ pressure perturbations. As a result, in the low q_s region the stationary zonal flow are dominant, while in high q_s region the zonal flow are oscillatory due to the coupling with the $(1,0)$ pressure perturbations. This result is reproduced in our gyrokinetic simulations as shown in fig. 11. But, the interest here is that the link between GAM amplitude and safety factor can be extended to the total plasma current value. From the five simulations with different total plasma current values, we plotted (fig. 12) the radial averaged rate of the GAM amplitude (G) and the steady zonal flow component (S) as a function of inverse total current. The fact that the q_s profile scales with the total current, and that GAM amplitude is proportional the q_s value, reflects on the linear dependence of G/S on the inverse total current.This brings us back to the scaling of the average ion conductivity χ_i with the total plasma current I_p. In section 4, it has been shown that χ_i is inversely proportional to I_p. This nonlinear result can now be understood in terms of interactions between zonal flow oscillation and ITG turbulence. In [7] it has been shown that, while the stationary zonal flows suppress the turbulence efficiently, fluctuations makes the suppression of the turbulence by the zonal

flows less effective. Increasing I_p reduces the GAM amplitude, the zonal flow behavior moves from oscillatory to stationary resulting in a lower χ_i.

7 Conclusions

A set of nonlinear electrostatic ITG turbulence simulations has been run with the global gyrokinetic PIC code ORB5. Two regimes can be distinguished in the nonlinear phase of the turbulence development. The first is characterized by a series of burst in the averaged radial heat flux, the second is characterized by a turbulent equilibrium set on place after the turbulence saturation. The burst phase can be explained in terms of temperature profile peaking and GAM oscillations. GAMs induce fluctuations in the zonal flow shearing rate. A burst starts in correspondence of a minimum of the sharing rate. The turbulence level locally grow and it drives the zonal flows until the shearing rate exceeds the linear growth rate. ITG turbulence and the associated heat transport are substantially reduced. After having been locally flattened, the temperature profile can peak again. The increased temperature gradient, and the lower shearing rate due to a minimum in the GAM oscillations, allow the turbulence to grow again and a new burst is started. The peak value of the ion conductivity is inversely proportional to the total plasma current as the GAM oscillations in the zonal flow. When the relaxation of the temperature profile leads the ITG modes close to the marginal stability, a new turbulent equilibrium is set on place. The ion conductivity and heat flux assumes a steady level while zonal flows oscillate at the GAM frequency. The average ion conductivity level and the GAM amplitude are inversely proportional to the total current.

The set of simulations gives a coherent picture in which the ion conductivity χ_i is linked to the amplitude of the zonal flow GAM oscillations through the total plasma current value (and correspondingly trough the safety factor profile). The safety factor, or the total current modulates the behavior of the zonal flows between stationary and oscillatory. A low total plasma current allows for oscillatory zonal flow which are less effective in shearing the turbulence leading to higher χ_i while a high value in the current lead to stationary zonal flow and a reduced χ_i. As a result, a linear scaling of χ_i with the total current can be established.

References

[1] X. Garbet, *Plasma Phys. Control. Fusion* **43**, A251 (2001).

[2] F. Romanelli, *Phys. Fluids B* **49**, 1018 (1989).

[3] H. A., M. Wakatani, *Phys. Rev. Lett.* **59**, 1581 (1987).

[4] K. Burrell, *Phys. Plasmas* **6**, 4418 (1999).

[5] Z. Lin, T. Hahm, W. Lee, W. Tang, R. White, *Science* **281**, 1835 (1998).

[6] N. Winsor, J. L. Johnson, D. J. M., *Phys. Fluids* **11**, 2448 (1968).

[7] T. S. Hahm, *et al.*, *Phys. Plasmas* **6**, 922 (1999).

[8] N. Miyato, Y. Kishimoto, *Phys. Plasmas* **11**, 5557 (2004).

[9] T. Hahm, *Phys. Fluids* **31**, 2670 (1988).

[10] A. Bottino, *et al.*, *Recent Advances in Nonlinear Gyrokinetic PIC Simulations in Tokamak Geometry* in *Theory of Fusion Plasmas, Int. Workshop* (Editrice Compositori, Societa' italiana di Fisica, Bologna, page 75, 2004).

[11] P. Angelino, *et al.*, *Geometrical Coupling of Zonal Flows on Electrostatic Microinstabilities* in *Theory of Fusion Plasmas, Int. Workshop* (Editrice Compositori, Societa' italiana di Fisica, Bologna, page 329, 2004).

[12] R. Hatzky, T.M. Tran, A. Könies *et al.*, *Phys. Plasmas* **9**, 898 (2002).

[13] S. Allfrey, R. Hatzky, *Comp. Phys. Commun.* **154**, 98 (2003).

[14] Y. Idomura, S. Tokuda, Y. Kishimoto, *Nucl. Fusion* **43**, 234 (2003).

[15] H. Lütjens, A. Bondeson, O. Sauter, *Comp. Phys. Commun.* **97**, 219 (1996).

[16] J. Wesson, *Tokamaks* (Clarendon Press, Oxford, 2nd edition, 1997).

[17] A. Bottino, PhD thesis No.**2938**, Ecole Polytechnique Fédérale de Lausanne (2004).

[18] R. E. Waltz, J. C. DeBoo, M. N. Rosenbluth, *Phys. Rev. Lett.* **65**, 2390 (1990).

[19] M. Fivaz, *et al.*, *Comp. Phys. Commun.* **111**, 27 (1998).

[20] M. N. Rosenbluth, H. F. L., *Phys. Rev. Lett.* **80**, 724 (1998).

[21] Z. Lin, T. S. Hahm, W. W. Lee, W. M. Tang, P. H. Diamond, *Phys. Rev. Lett.* **83**, 3645 (1999).